J|A|C|S
ARTICLES
Published on Web 04/04/2006

A Solid-State NMR Study of the Dynamics and Interactions of Phenylalanine Rings in a Statherin Fragment Bound to Hydroxyapatite Crystals

James M. Gibson,[†,#] Jennifer M. Popham,[‡] Vinodhkumar Raghunathan,[†,‡] Patrick S. Stayton,*[,†] and Gary P. Drobny*[,‡]

Contribution from the Departments of Bioengineering and Chemistry, University of Washington, Seattle, Washington 98195

Received October 11, 2005; E-mail: stayton@u.washington.edu; drobny@chem.washington.edu

Abstract: Extracellular matrix proteins regulate hard tissue growth by acting as adhesion sites for cells, by triggering cell signaling pathways, and by directly regulating the primary and/or secondary crystallization of hydroxyapatite, the mineral component of bone and teeth. Despite the key role that these proteins play in the regulation of hard tissue growth in humans, the exact mechanism used by these proteins to recognize mineral surfaces is poorly understood. Interactions between mineral surfaces and proteins very likely involve specific contacts between the lattice and the protein side chains, so elucidation of the nature of interactions between protein side chains and their corresponding inorganic mineral surfaces will provide insight into the recognition and regulation of hard tissue growth. Isotropic chemical shifts, chemical shift anisotropies (CSAs), NMR line-width information, ^{13}C rotating frame relaxation measurements, as well as direct detection of correlations between ^{13}C spins on protein side chains and ^{31}P spins in the crystal surface with REDOR NMR show that, in the peptide fragment derived from the N-terminal 15 amino acids of salivary statherin (i.e., SN-15), the side chain of the phenylalanine nearest the C-terminus of the peptide (F14) is dynamically constrained and oriented near the surface, whereas the side chain of the phenylalanine located nearest to the peptide's N-terminus (F7) is more mobile and is oriented away from the hydroxyapatite surface. The relative dynamics and proximities of F7 and F14 to the surface together with prior data obtained for the side chain of SN-15's unique lysine (i.e., K6) were used to construct a new picture for the structure of the surface-bound peptide and its orientation to the crystal surface.

Introduction

The regulation of biomineralization in teeth, bone, sea urchin spines, mollusks' shells, and mineralized algae together with the material properties of the mineral component of these structures are all controlled by proteins.[1−10] In humans, osteopontin, bone silaoprotein, and other acidic protein components of the extracellular matrix (ECM) play key roles in promoting or inhibiting the growth of the apatitic mineral component of bone and tooth enamel. Fundamental to understanding the functional role of ECM proteins in hard tissue repair and modeling is knowledge of the structural and dynamical basis for how these macromolecules interact with inorganic surfaces.

In addition to investigating the molecular-level basis for the recognition of biomineral surfaces and the control of hard tissue growth by proteins, the development of materials with enhanced biocompatibility is a major focus of the materials and tissue engineering communities. Answers to such fundamental questions, such as what is the structure of a surface-bound protein, what part of a protein interacts with the surface, how is the protein oriented on the surface, and what role might molecular dynamics play in protein function, continue to elude the fields of bioengineering, medicine, and dentistry, mainly because few high-resolution structure−function studies have been performed on protein−mineral complexes.

Salivary statherin is a 43 amino acid proline and tyrosine-rich phosphopeptide found in the sub-mandibullar saliva. Statherin has the dual function of inhibiting both nucleation and crystal growth of hydroxyapatite [$Ca_{10}(PO_4)_6(OH)_2$, (HAP)] in the oral environment.[11] Statherin also acts as a boundary lubricant and has been found to have bacterial binding domains for *Porphyromonas gingivalis*[12] and *Actinomyces viscosus*.[13] The

[†] Department of Bioengineering.
[‡] Department of Chemistry.
[#] Current address: Department of Chemistry and Chemical Biology, Rensselaer Polytechnic Institute, Troy, NY 12180.

(1) Berman, A.; Addadi, L.; Kvick A.; Leiserowitz, L.; Nelson, M.; Weiner, S. *Science* **1990**, *250*, 664−667.
(2) Berman, A.; Addadi, L.; Weiner, S. *Nature* **1988**, *331*, 546−548.
(3) Weiner, S. In *CRC Crit. Rev. Biochem.* **1985**, *20*, 365−408.
(4) Johnsson, M.; Levine, M. J.; Nancollas, G. H. *Crit. Rev. Oral Biol. Med.* **1993**, *4*, 371−378.
(5) Richardson, C. F.; Johnsson, M.; Raj, P. A.; Levine, M. J.; Nancollas, G. H. *Arch. Oral. Biol.* **1993**, *38*, 997−1002.
(6) Fujisawa, R.; Wada, Y.; Nodasaka, Y.; Kuboki, Y. *Biochim. Biophys. Acta: Protein Struct. Mol. Enzymol.* **1996** *1292*, 53−60.
(7) Goldberg, H. A.; Li, M.; Warner, K. J.; Hunter, G. K. *J. Dent. Res.* **1996**, *75*, 914.
(8) Hunter, G. K.; Goldberg, H. A. *J. Dent. Res.* **1994**, *73*, 282.
(9) Hunter, G. K.; Goldberg, H. A. *Biochem. J.* **1994**, *302*, 175−179.
(10) Fincham, A. G.; Moradian-Oldak, J.; Simmer, J. P. *J. Struct. Biol.* **1999**, *126*, 270−299.
(11) Schlesinger, D. H.; Hay, D. I. *J. Biol. Chem.* **1977**, *252*, 1689−1695.

10.1021/ja056731m CCC: $33.50

structure of statherin has been studied by solution-state NMR,[14] solid-state NMR,[15−20] and circular dichroism,[21−23] and its affinity for HAP surfaces has been determined by binding isotherms.[24,25] The primary structure of statherin is

1 Asp-pSer-pSer-Glu-Glu-Lus-Phe-Leu-Arg-Arg-Ile-Gly-Arg-Phe-Gly 15

16 Tyr-Gly-Tyr-Gly-Pro-Tyr-Gln-Pro-Val-Pro-Glu-Gln-Pro 28

29 Leu-Tyr-Pro-Gln-Pro-Tyr-Gln-Pro-Gln-Tyr-Gln-Gln-Tyr-Thr-Phe 43

where the three-letter amino acid abbreviations are used and the lower case p in front of the serine residues indicates a phosphorylation of those amino acids. For the remainder of this paper, we will use the single letter amino acid abbreviations and the numbered position from the N-terminus to designate the amino acid residues being studied (e.g., K6 or F7).

Solid-state NMR studies previously performed on the full-length native protein and on a 15 amino acid N-terminal peptide fragment (SN-15) measured both the structure and dynamics of the N-terminal HAP recognition domain in the bound state. The model surface used in all these studies was synthetically prepared HAP. The major difference between the enamel apatite and mineral hydroxyapatite is the presence of 3 wt % CO_3^{2-} in the enamel apatite. The actual positions of the carbonate ions cannot be directly determined because the enamel apatite crystals are too small for single-crystal structure determination.[26] The high surface area of the HAP used ensures that the crystallites of HAP used in the study are small enough to mimic enamel apatite, while providing some control over the composition.

Double Quantum Dipolar Recoupling with a Windowless Sequence (DQ-DRAWS) NMR,[27] DRAWS NMR,[28] and Rotational-Echo-Double-Resonance (REDOR) NMR[29−31] measurements were used to characterize and contrast the structure of both the full-length statherin protein and the SN-15 fragment. These measurements demonstrated that the full-length protein is α-helical from pS2 to G12,[20] whereas SN-15 is in an extended conformation from pS3 to F7 and α-helical from residues L8 to G12.[18]

Dynamics along the backbone of both statherin and SN-15 were examined to determine the degree to which the protein and peptide were immobilized by interactions with the HAP surface.[19,20] In these studies, both chemical shift anisotropy (CSA) measurements and ^{13}C $T_{1\rho}$ measurements were performed on the backbone ^{13}C carbonyl spins. In both cases, the backbone carbonyl ^{13}C CSA and the ^{13}C $T_{1\rho}$ decreases as one moves from the N-terminus toward the C-terminus, indicating that the acidic pentapeptide region is closely associated with the HAP, whereas the rest of the peptide is less strongly associated with HAP. ^{13}C $T_{1\rho}$ measured at all six positions (pS2, pS3, F7, L8, I11, and G12) were almost identical in both SN-15 and statherin, suggesting a similar trend in correlation times for backbone motions in both systems. On the other hand, the CSA measurements, which are indicators of dynamic amplitudes, were not the same for SN-15 and statherin. In the case of SN-15, the backbone carbonyl CSA correlated well with the ^{13}C $T_{1\rho}$ values as one moved from the N-terminus to the C-terminus, indicating an increase in amplitude of motion along with an increase in the frequency of motion.[19] Statherin, in contrast, demonstrated almost no change in carbonyl ^{13}C CSAs from amino acids at the N-terminus to amino acids at the C-terminus. The lack of amplitude was attributed to restriction of spatial motion by the presence of the larger protein on top of the 15 amino acid fragment. It was suggested that the mobility of statherin could allow it to block more nucleation sites than a rigidly bound protein and might account for the observation that statherin required lower than expected surface coverage when compared to a theoretically determined surface area of a fixed globular protein.[20,24]

To further our understanding of the orientation and binding of statherin and SN-15 to HAP, careful examination of the side chain interactions with the surface is required. Previously, we used $^{15}N\{^{31}P\}$ REDOR NMR to demonstrate that the K6 in the peptide fragment interacted with the HAP surface.[32] Here, we examine and compare the phenylalanine side chains, of which there are two in the peptide sequence. Among the hydrophobic amino acids, phenylalanine has been shown to have the strongest binding affinity for HAP and is the strongest growth inhibitor for HAP.[33] In view of these facts, it has been suggested that phenylalanine acts as an electron donor to the HAP surface through its aromatic ring. This observation of a weak bond between the singular phenylalanine amino acid and HAP provides the motivation for our study of interactions between phenylalanine side chains in SN-15 and HAP.

In addition to the orientation of the peptide side chains, measuring dynamics of protein side chains yields information about their behavior in the binding process. Solid-state NMR $T_{1\rho}$ and CSA measurements have been frequently used to probe the dynamics of amino acids, proteins, and polymers,[34−40] and

(12) Amano, A.; Kataoka, K.; Raj, P. A.; Genco, R. J.; Shizukuishi, S. *Infect. Immun.* **1996**, *64*, 4249−4254.
(13) Ramasubbu, N.; Thomas, L. M.; Bhandary, K. K.; Levine, M. J. *Crit. Rev. Oral Biol. Med.* **1993**, *4*, 363−370.
(14) Elgavish, G. A.; Hay, D. I.; Schlesinger, D. H. *Int. J. Pept. Protein Res.* **1984**, *23*, 230−234.
(15) Stayton, P. S.; Drobny, G. P.; Shaw, W. J.; Long, J. R.; Gibert, M. *Crit. Rev. Oral Biol. Med.* **2003**, *14*, 370−376.
(16) Drobny, G. P.; Long, J. R.; Karlsson, T.; Shaw, W.; Popham, J.; Oyler, N.; Bower, P.; Stringer, J.; Gregory, D.; Mehta, M.; Stayton, P. S. *Annu. Rev. Phys. Chem.* **2003**, *54*, 531−571.
(17) Long, J. R.; Dindot, J. L.; Zebroski, H.; Kiinhe, S.; Clark, R. H.; Campbell, A. A.; Stayton, P. S.; Drobny, G. P. *Proc. Natl. Acad. Sci. U.S.A.* **1998**, *95*, 12083−12087.
(18) Shaw, W. J.; Long, J. R.; Dindot, J. L.; Campbell, A. A.; Stayton, P. S.; Drobny, G. P. *J. Am. Chem. Soc.* **2000**, *122*, 4939−4946.
(19) Shaw, W. J.; Long, J. R.; Campbell, A. A.; Stayton, P. S.; Drobny, G. P. *J. Am. Chem. Soc.* **2000**, *122*, 7118−7119.
(20) Long, J. R.; Shaw, W. J.; Stayton, P. S.; Drobny, G. P. *Biochemistry* **2001**, *40* 15451−15455.
(21) Douglas, W. H.; Reeh, E. S.; Ramasubbu, N.; Raj, P. A.; Bhandary, K. K.; Levine M. J. *Biochem. Biophys. Res. Commun.* **1991**, *180*, 91−97.
(22) Gururaja, T. L.; Ramasubbu, N.; Levine, M. J. *Lett. Pept. Sci.* **1996**, *3*, 79−88.
(23) Naganagowda, G. A.; Gururaja, T. L.; Levinem M. J. *J. Biomol. Struct. Dyn.* **1998**, *16*, 91−107.
(24) Moreno, E. C.; Kresak, M.; Hay, D. I. *Calcif. Tissue Int.* **1984**, *36*, 48−59.
(25) Raj, P. A.; Johnsson, M.; Levine, M. J.; Nancollas, G. H. *J. Biol. Chem.* **1992**, *267*, 5968−5976.
(26) Wilson, R. M.; Elliot, J. C.; Dowker, S. E. P. *Am. Mineral.* **1999**, *84*, 1406−1414.
(27) Gregory, D. M.; Wolfe, G. M.; Jarvie, T. P.; Shiels, J. C.; Drobny, G. P. *Mol. Phys.* **1996**, *89*, 1835−1849.
(28) Gregory, D. M.; Mitchell, D. J.; Stringer, J. A.; Kiihne, S.; Shiels, J. C.; Callahan, J.; Mehta, M. A.; Drobny, G. P. *Chem. Phys. Lett.* **1995**, *246*, 654−663.
(29) Gullion, T.; Schaefer, J. *J. Magn. Reson.* **1989**, *81* 196−200.
(30) Gullion, T.; Schaefer, J. *Adv. Magn. Reson.* **1989**, *13*, 57−83.
(31) Gullion, T. *Conc. Magn. Reson.* **1998**, *10*, 277−289.
(32) Gibson, J. M.; Raghunathan, V.; Popham, J. M.; Stayton, P. S.; Drobny, G. P. *J. Am. Chem. Soc.* **2005**, *127*, 9350−9351.
(33) Koutsopoulos, S.; Dalas, E. *Langmuir* **2000**, *16*, 6739−6744.
(34) Schaefer, J.; Stejskal, E. O.; Buchda, R. *Macromolecules* **1977**, *10*, 384−405.

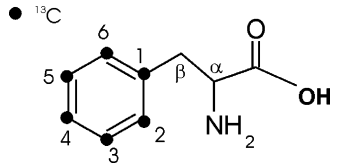

Figure 1. A chemical drawing of phenylalanine is shown, with the incorporated ring labels noted.

the motions of aromatic rings have been extensively studied by solid-state NMR in a variety of systems.[41−44] In free proteins, dynamic solid-state NMR studies demonstrate that the aromatic rings of phenylalanine almost always undergo 2-fold "π-flipping" motions.[41] Here, we determine the detailed dynamics of phenylalanine side chains in SN-15 peptide adsorbed onto HAP crystals. By correlating side chain dynamic data with side chain-to-surface distance measurements, we probe the degree to which phenylalanine side chain dynamics report the local environments of the F7 and F14 side chains at the HAP surface.

To determine the orientation of the SN-15 peptide on the HAP surface, we use $^{13}C\{^{31}P\}$ REDOR to measure distances from ^{13}C spins in the side chains of F7 and F14 to ^{31}P spins in the HAP surface. REDOR has been used previously to measure secondary structure in free proteins[45−48] and proteins bound to surfaces[15,16,18,20] as well as recently to measure distances from organic matrices to crystal surfaces.[32,49,50] We also use ^{13}C $T_{1\rho}$, CSA, and line-width measurements to investigate the motion of the side chains of F7 and F14 in SN-15, and we compare and contrast these motions with similar measurements of the dynamics of backbone carbonyl ^{13}C spins, described previously.[19]

Materials and Methods

Materials. Protected amino acids and Fmoc-Gly-Wang resin were purchased from Calbiochem-Novabiochem Corp. (San Diego, CA). [Ring-$^{13}C_6$] L-phenylalanine was purchased from Cambridge Isotope Laboratories, Inc. (Andover, MA). The labeling scheme for phenylalanine is shown in Figure 1. HAP (55 m^2/g) was synthesized by Allison Campbell at Pacific Northwest National Lab as published previously.[18]

Peptide Synthesis and Characterization. Both [ring-$^{13}C_6$]-labeled phenylalanine SN-15 samples were prepared as follows. [Ring-$^{13}C_6$] L-phenylalanine was FMOC protected using standard procedures.[51] From a preloaded Fmoc-Gly-Wang resin (substitution 0.60 mmol/g), the SN-15 peptide was synthesized on a Rainin PS3 automated solid-phase peptide synthesizer (Protein Technologies, Inc.), where the solvent was *N*,*N*-dimethylformamide (DMF), the activator was 0.4 M *N*-methyl morpholine in DMF, and the deprotector was 20% (v/v) piperidine in DMF. The acidic portion of SN-15 (D1 to K6) was double coupled, while the rest of the peptide was built through single couplings. The peptide was cleaved from the resin using a 9.5 TFA:0.25 H_2O:0.25 TIS (triisopropylsilane) solution following Method 3−18 described in the Novabiochem 2002/3 catalog.[52] Using a Waters HPLC C-18 reverse phase column, the peptide was purified with an acetonitrile/water solvent system with 0.1% TFA, eluting at 35.4% acetonitrile, lyophilized, and then analyzed by MALDI mass spectrometry to establish composition and purity.

Peptide Adsorption to HAP. SN-15 was physisorbed to HAP by mixing a solution composed of 0.05 mM of peptide in a phosphate buffer with about 100 mg of HAP (55 m^2/g). The pH of the mixture was adjusted to 7.4 with NaOH and HCl. The phosphate buffer was 100 mM NaCl, 40 mM KCl, 1.4 mM KH_2PO_4, and 4.3 mM Na_2HPO_4. After 4 h of mixing, the unbound peptide was separated from the peptide−HAP complex though centrifugation. The peptide−HAP sample was washed several times with buffer and was packed in the rotor for solid-state NMR studies. It was later lyophilized after hydrated data were acquired.

NMR Experiments. Solid-state NMR experiments were performed on two spectrometers. CPMAS of the free phenylalanine, free F7 peptide, and both bound peptides, REDOR of the free F7 peptide, and all $T_{1\rho}$ experiments were performed on a home-built spectrometer attached to a 11.7 T superconducting magnet and operating at Larmor frequencies of 500.32 MHz for ^1H, 202.53 MHz for ^{31}P, and 125.74 MHz for ^{13}C. Samples were spun at rates of 16 000, 8000, or 4000 Hz and regulated to ± 1 Hz by a home-built spin-rate controller. CPMAS of the free and bound F14 peptide and REDOR of the free F14 peptide were performed using a 4 mm HXY triple-resonance Varian/Chemagnetics magic-angle spinning probe on a Chemagnetics spectrometer attached to a 7.1 T superconducting magnet operating at Larmor frequencies of 300.16 MHz for ^1H, 121.44 MHz for ^{31}P, and 75.44 MHz for ^{13}C. NMR experiments were performed at 7.1 T with a 5 mm HXY triple-resonance Varian/Chemagnetics magic-angle spinning probe, spinning at 8000 $\pm$ 1 Hz. REDOR measurements on the bound, hydrated peptides at room temperature were performed on both spectrometers at 8000 $\pm$ 1 Hz. CPMAS and REDOR experiments on the hydrated and lyophilized samples were performed at both room temperature and at −30 °C, controlled with an FTS cooler. $T_{1\rho}$ experiments were performed using an FTS cooler under all conditions in order to maintain temperatures at either 20 or −30 °C.

For all samples and spectrometers, the version of REDOR with only a single refocusing pulse and multiple π-pulses on the dephasing channel was used with XY-8 phase cycling on the dephasing channel, as shown in Figure 2a. This sequence was chosen to reduce SEDRA-type interactions between multiple ^{13}C labels on the observe channel.[53−56] Because ^{13}C homonuclear *J*-coupling can create inaccuracies over long dephasing times,[57,58] REDOR dephasing was restricted to 5 ms. Pulse lengths were as follows: 3.5 μs for the ^1H $\pi/2$ pulse, 200 μs for the contact time, 15 μs for the ^{13}C π pulses, and 12.5 μs for the ^{31}P π

(35) Fernandez, V. L.; Reimer, J. A.; Denn, M. M. *J. Am. Chem. Soc*. **1992**, *114*, 9634−9642.
(36) Gerard, A.; Laupretre, F.; Monnerie, L. *Macromolecules* **1993**, *26*, 3313−3318.
(37) Garbow, J.; Goetz, J.; Asrar, J. *Macromolecules* **1998**, *31*, 3925−3930.
(38) Klein, P. G.; Evans, B. W.; Ward, I. M. *Polymer* **1998**, *39*, 3349−3354.
(39) Maxwell, A. S.; Ward, I. M.; Laupretre, F.; Monnerie, L. *Polymer* **1998**, *39*, 6835−6849.
(40) Wei, Y.; Lee, D.-K., Ramamoorthy, A. *J. Am. Chem. Soc.* **2001**, *123*, 6118−6126.
(41) Hiraoki, T.; Kogame, A.; Nishi, N.; Tsutsumi, A. *J. Mol. Struct*. **1998**, *441*, 243−250.
(42) Frey, M. H.; DiVerdi, J. A.; Opella, S. J. *J. Am. Chem. Soc*. **1985**, *107*, 7311−7315.
(43) Gall, C. M.; DiVerdi, J. A.; Opella, S. J. *J. Am. Chem. Soc*. **1981**, *103*, 5039−5043.
(44) Schaefer, J.; Stejskal, E. O.; McKay, R. A.; Dixon, W. T. *J. Magn. Reson*. **1984**, *57*, 85−92.
(45) Balbach, J. J.; Ishii, Y.; Antzutkin, O. N.; Leapman, R. D.; Rizzo, N. W.; Dyda, F.; Reed, J.; Tycko, R. *Biochemistry* **2000**, *39*, 13748−13759.
(46) Ladizhansky, V.; Veshtort, M.; Griffin, R. G. *J. Magn. Reson*. **2002**, *154*, 317−324.
(47) Gordon, D. J.; Balbach, J. J.; Tycko, R.; Merdith, S. C. *Biophys. J*. **2004**, *86*, 428−434.
(48) Bernard, G. M.; Miskolzie, M.; Kotovych, G.; Wasylishen, R. E. *Can. J. Chem.: Rev. Can. Chim.* **2004**, *82*, 1554−1563.
(49) Shaw, W. J.; Campbell, A. A.; Paine, M. L.; Snead, M. L. *J. Biol. Chem*. **2004**, *279*, 40263−40266.
(50) Jaeger, C.; Groom, N. S.; Bowe, E. A.; Horner, A.; Davies, M. E.; Murray, R. C.; Duer, M. J. *Chem. Mater*. **2005**, *17*, 3059−3061.
(51) Kates, S.; Albericio, F. *Solid-Phase Synthesis: A Practical Guide*; Marcel Dekker: New York, 2000.
(52) Novabiochem catalog; pp 3.14−3.19, 2002−2003.
(53) Gullion, T.; Vega, S. *Chem. Phys. Lett.* **1992**, *194*, 423−428.
(54) Schaefer, J. *J. Magn. Reson*. **1999**, *137*, 272−275.
(55) Jaroniec, C. P.; Tongue, B. A.; Herzfeld, J.; Griffin, R. G. *J. Am. Chem Soc*. **2001**, *123*, 3507−3519.
(56) Mehta, A. K.; Segelski, L.; O'Connor, R. D.; Schaefer, J. *J. Magn. Reson*. **2003**, *163*, 182−187.
(57) Jaroniec, C. P.; Tongue, B. A.; Rienstra, C. M.; Herzfeld, J.; Griffin, R. G. *J. Am. Chem. Soc.* **1999**, *121*, 10237−10238.
(58) Vogt, F. G.; Gibson, J. M.; Mattingly, S. M.; Mueller, K. T. *J. Phys. Chem. B* **2003** *107*, 1272−1283.

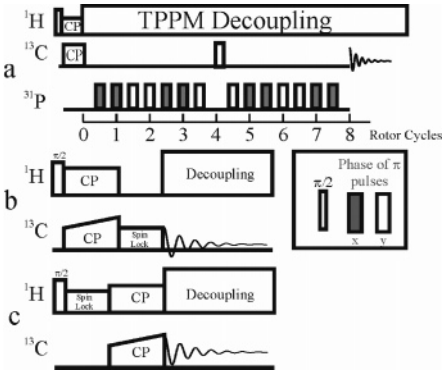

Figure 2. (a) The REDOR pulse sequence used in this study, with one pulse on the observed (^{13}C) channel, and pulses every half-rotor period on the dephasing (^{31}P) channel are shown. (b) The ^{13}C $T_{1\rho}$ pulse sequence is depicted. (c) The ^{1}H $T_{1\rho}$ pulse sequence, with the magnetization detected through ^{13}C spins after cross-polarization, is pictured.

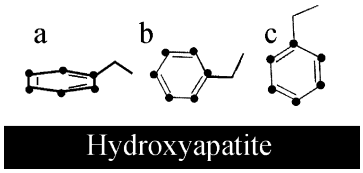

Figure 3. Three different orientations of the phenyl ring with respect to the HAP surface were considered: (a) the ring plane is parallel to the HAP surface; (b) a line perpendicular to the C_2-C_3 and C_5-C_6 bonds is also perpendicular to the HAP surface; and (c) a line from C_1 to C_4 is perpendicular to the HAP surface.

pulses. TPPM decoupling[59] was utilized throughout all REDOR experiments and during the acquisition of CPMAS and $T_{1\rho}$ experiments at a field of 100 kHz during the pulse sequence and acquisition. A pulse delay of 5 s was used in most experiments other than those involving a bound, lyophilized F7-labeled sample, which required a 10 s pulse delay, and free phenylalanine, which required a 45 s pulse delay.

In the ^{13}C $T_{1\rho}$ experiments (Figure 2b), the spin-lock time was varied from 1 to 5 ms, and in the ^{1}H $T_{1\rho}$ experiments (Figure 2c), the spin-lock time was varied from 100 to 500 μs. The same ^{1}H $\pi/2$ pulse and CP times described for the REDOR experiments were also utilized for the $T_{1\rho}$ experiments. Spin-locking fields of 46 kHz for the ^{13}C spins and 30 kHz for the ^{1}H spins were used for both the CP experiments and the $T_{1\rho}$ experiments, with ramped CP on the ^{13}C spin from 42 to 50 kHz for the 8 and 16 kHz experiments, and ramped CP on the ^{13}C spin from 30 to 38 kHz experiments for the 4 kHz spinning experiments.

Simulations and Data Fitting. Theoretical REDOR curves were calculated using the simulation program SIMPSON.[60] Simulations were performed using the direct algorithm, along with a set of 54 Euler angles, specified by the Zaremba−Conroy−Wolfsberg[61,62] scheme, and 10 γ angles. For the sake of simplicity, simulations were performed with only a single ^{31}P spin. The short dephasing time necessitated by the *J*-coupling also allows us to ignore any ^{31}P−^{31}P homonuclear dipolar coupling contributions to the REDOR dephasing curve. Three different orientations of the phenylalanine ring relative to the planar HAP surface were considered, as shown in Figure 3. In the first case, the ring was oriented parallel to the HAP surface. In the second case, the ring was oriented perpendicular to the HAP surface such that a line drawn perpendicular to the C_2-C_3 and C_5-C_6 bonds is also perpendicular to the HAP surface. In the third case, the ring was oriented perpendicular to the surface such that a line drawn from C_1 to C_4 is also perpendicular to the HAP surface. For a single ^{31}P spin, the spin was assumed to be oriented such that a line drawn from the center of mass of the phenyl ring to the ^{31}P spin is perpendicular to the HAP surface. Simulated data were then based on an average of the five different resulting REDOR curves. Reduced χ^2 values were calculated with the same method as reported by Karlsson et al.[63] in order to determine the error limits of the calculated distances.

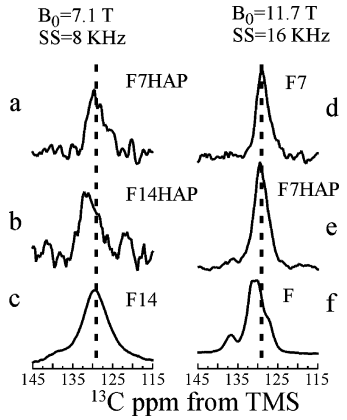

Figure 4. ^{13}C CPMAS spectra at room temperature for free phenylalanine, free peptide, and peptide bound to HAP are shown. The dashed line at 130 ppm represents the center of mass of the peak for C_2 to C_6 for both free peptides.

^{13}C $T_{1\rho}$ and ^{1}H $T_{1\rho}$ experiments were fit to a single exponential, creating an average $T_{1\rho}$ time over all five observable ^{13}C spins, seen as a single peak. CSA values were calculated using Klaus Eichele's Herfzfeld−Berger analysis program.[64] Error limits on the CSA values were set by calculating the value at both 4 kHz spinning and 8 kHz spinning, as higher anisotropic values were generally calculated from the 8 kHz spectra.

Results

^{13}C CPMAS Spectra of Free and HAP-Bound SN-15. In Figure 4 are shown the ^{13}C CPMAS spectra of free SN-15 peptides labeled with ^{13}C on the phenyl groups of F7/F14 and similarly labeled SN-15 peptides bound to HAP. These spectra are also compared to a CPMAS spectrum for uniformly ^{13}C-labeled free phenylalanine. In all cases, the C_2 through C_6 carbon atoms are represented by a single peak, although in free phenylalanine, a shoulder is present that is assigned to C_4. Additionally, in the case of free phenylalanine, a resolved peak was observed corresponding to C_1. The C_1 peaks have smaller amplitudes than other phenyl ^{13}C spins in the CPMAS spectra of the free peptide probably because the ring motion creates poor CP efficiency for the single unprotonated ^{13}C spin. Although C_1 peaks were observed in the one-pulse ^{13}C MAS spectra (not shown) for both free peptides, neither one-pulse ^{13}C MAS nor ^{13}C CPMAS spectra for the bound peptides had sufficient S/N for observation of the C_1 peak. Maximum efficiency for the protonated ^{13}C spins was obtained at extremely short mixing times.

Slow-spinning spectra for the bound samples and the free amino acid are pictured in Figure 5 to demonstrate the sideband pattern. Data including the line widths of the peak representing C_2 through C_6, the isotropic peak values, and the observed CSAs

(59) Bennett, A. E.; Rienstra, C. M.; Auger, M.; Lakshmi, K. V.; Griffin, R. G. *J. Chem. Phys.* **1995**, *103*, 6951−6958.
(60) Bak, M.; Rasmussen, J. T.; Nielsen, N. C. *J. Magn. Reson.* **2000**, *147*, 296−330.
(61) Conroy, H. *J. Chem. Phys.* **1967**, *47*, 5307−5318.
(62) Cheng, V. B.; Suzukawa, H. H.; Wolfsberg, M. *J. Chem. Phys.* **1987**, *59*, 3992−3999.
(63) Karlsson, T.; Popham, J. M.; Long, J. R.; Oyler, N.; Drobny, G. P. *J. Am. Chem. Soc.* **2003**, *125*, 7394−7407.
(64) Eichele, K.; Wasylishen, R. E. *HBA*, version 1.5; Dalhousie University, 2005.

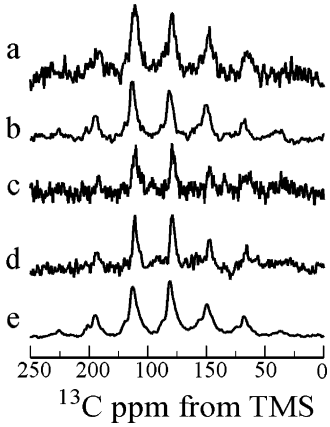

Figure 5. ^{13}C CPMAS spectra at 4 kHz are shown for (a) the lyophilized F14 sample bound to HAP at 20 °C, (b) the hydrated F14 sample bound to HAP at 20 °C, (c) the lyophilized F7 sample bound to HAP at 20 °C, (d) the hydrated F7 sample bound to HAP at 20 °C, and (e) free phenylalanine. Hydrated data at −30 °C were similar and are not shown.

Table 1. Chemical Shift Measurements for Free Phenylalanine, Free Peptide, and Bound Peptide under Different Conditions

sample	temp	condition	center of mass isotropic chemical shift (ppm)	line width (ppm)	CSA (ppm)
F	rt	lyophilized	131	6.5	160 ± 20
free F7	rt	lyophilized	130	4.9	150 ± 20
bound F7	rt	hydrated	130	3.0	150 ± 20
bound F7	−30 °C	hydrated	130	4.0	150 ± 20
bound F7	rt	lyophilized	130	4.4	150 ± 20
free F14	rt	lyophilized	130	6.9	150 ± 20
bound F14	rt	hydrated	132	5.6	160 ± 20
bound F14	−30 °C	hydrated	132	6.2	160 ± 20
bound F14	rt	lyophilized	132	6.6	160 ± 20

Table 2. ^{13}C $T_{1\rho}$ Measurements for the Bound Peptide Samples

sample	temp (°C)	sample condition	^{13}C $T_{1\rho}$ (ms)
bound F7	20	hydrated	5.6 ± 0.5
bound F7	−30	hydrated	4.8 ± 0.5
bound F7	20	lyophilized	3.5 ± 0.5
bound F14	20	hydrated	5.3 ± 0.3
bound F14	−30	hydrated	7.5 ± 0.5
bound F14	20	lyophilized	10 ± 1.5

are shown in Table 1. Asymmetry values were not calculated because sidebands in the slow-spinning spectra have a large contribution from the ^{13}C−^{13}C dipolar couplings and the fast-spinning spectra do not contain enough sidebands for an accurate measurement of the asymmetry parameter.

Rotating Frame Relaxation Experiments. Average ^{13}C $T_{1\rho}$ values for both HAP-bound peptides under different conditions are listed in Table 2.

^{13}C{^{31}P} REDOR Experiments. ^{13}C{^{31}P} REDOR was performed on both unbound peptide samples to gauge the chance of interference from dipolar coupling between the pS side chains and the F side chains. In this case, neither sample showed any dephasing to 5 ms, suggesting the distance between the ^{31}P spin on the pS side chains to a ^{13}C spin on the phenylalanine exceeds 6.5 Å. This limit is based on the fact that a 6.5 Å distance results in a 41 Hz dipolar coupling, which yields an S/S_0 value of 0.95 at 5 ms of dephasing. ^{13}C{^{31}P} REDOR was also performed on both bound peptides. In the case of the F7-labeled sample, no dephasing was seen over the same 5 ms limit as for the unbound sample. This observation was true for all three conditions of the peptide. REDOR data on the F14-labeled sample bound to HAP showed rapid dephasing, as indicated in Figure 6a. Again, similar data were obtained under all three experimental conditions.

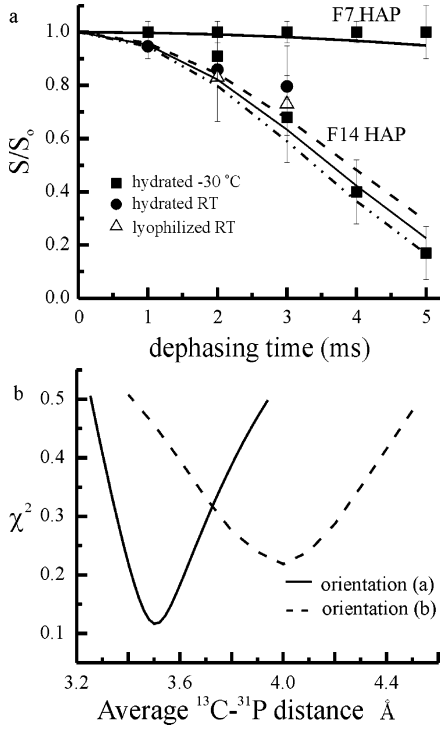

Figure 6. REDOR analysis of both samples bound to HAP is shown. In (a), the experimental data and best simulated fits are shown for both samples. In (b), a χ^2 map is shown for the F14 sample based on the orientations pictured in Figure 3.

A χ^2 plot of the fits based on the geometries described earlier is shown in Figure 6b. Using the geometry pictured in Figure 3a and a single ^{31}P spin, the best fit results in an average ^{13}C−^{31}P distance of 3.85 ± 0.15 Å. Clearly, a larger ^{31}P network is present due to the HAP, but further simulations suggest that we are only underestimating the distance by about 0.5−1 Å. A recent paper also explicitly modeled multiple ^{31}P spin dephasers and indicated this is a reasonable error estimate.[65] The lower limit on the F7 distance of 6.5 Å is also likely underestimated by a similar amount.

Discussion

Surface Interactions. ^{13}C{^{31}P} REDOR measurements show that the F7 side chain is least 6.5 Å away and probably more than 7 Å away from any single ^{31}P on the HAP surface upon binding and is therefore oriented away from the surface and not involved in any interaction between the peptide and the HAP surface. The F14 side chain, on the other hand, demonstrates a clear dephasing pattern under all conditions, and its phenyl ring is approximately 4.3−4.8 Å away from the HAP surface. As mentioned in the Introduction, free phenylalanine has been shown to adsorb onto HAP.[33] It was suggested that phenylalanine weakly π-bonds to HAP, and as a result, it would be expected that the phenyl ring lies flat on the HAP surface. Our REDOR study of the F14 side chain is consistent with this

(65) Goobes, G.; Raghunathan, V.; Louie, E. A.; Gibson, J. M.; Olsen, G. L.; Drobny, G. P. *Solid-State Nucl. Magn. Reson.* **2006**, *29*, 242−250.

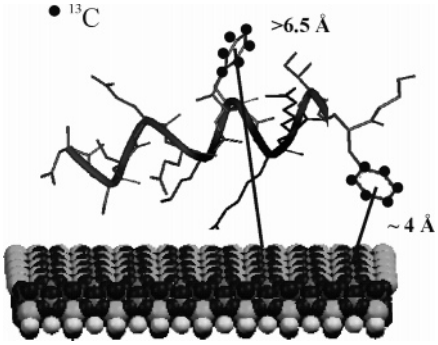

Figure 7. A modified SN-15 model with peptide bound to HAP is presented, in which the C-terminus loses its α-helicity, and both the K6 and F14 side chains are within close proximity to the HAP surface.

geometry. The distance in this case is further than what is likely a hydrogen bond between the K6 side chain and a surface phosphate group reported in a prior publication,[32] suggesting that the interaction between the F14 side chain and the HAP surface is significantly weaker than the interaction between the K6 side chain and the HAP surface, as expected. In addition, the backbone motion described in earlier publications also suggests that K6 would likely be a stronger candidate for interaction with the HAP surface than F14. The combined results of the prior backbone data,[18,19] prior side chain data,[32] and these data suggest that the F14 phenyl ring is close to the surface, but only weakly interacting when compared with polar side chains at the N-terminus.

In addition to measuring the side chain interactions, the REDOR allows us to further refine the proposed structure for the bound peptide. In a perfect α-helix, side chains at the *i* and $i + 7$ positions should be oriented in the same direction. Therefore, in SN-15, one phenylalanine side chain oriented away from the surface and one phenylalanine oriented toward the surface is not consistent with perfect helical structure. Prior studies of the secondary structure of SN-15 were only performed out to the 12 amino acid in the sequence, and through the DRAWS experiment, it was shown that the helix at I11G12 is already extended versus the helix at F7L8, meaning that it is likely that the peptide loses its helicity at the C-terminus.[18] Proteins in solutions have often been shown to be in random coil near the N-terminus, α-helical in the middle, and random coil again at the C-terminus,[66] therefore our findings here are consistent with that type of model. A new picture that accounts for α-helical structure between residues F7 and G12 allows the pS2, pS3, K6, and F14 side chains to be oriented toward the surface and allows the F7 side chain to be oriented away from the surface, as shown in Figure 7.

In addition to the aforementioned REDOR measurements allowing high-resolution measurements of distances between the side chains and the HAP surface, other measurements were used to indicate general proximity to the surface. Previously, Fernandez et al. had used chemical shift changes to indicate binding to the surface.[35] Additionally, we noted both an observed REDOR effect and an isotropic chemical shift change upon binding in our prior study of the K6 side chain.[32] The isotropic chemical shift of the F14 ring increased by 2 ppm upon binding, whereas the isotropic chemical shift of the F7 ring remained constant upon binding.

Dynamics of the Phenyl Rings. In addition to measuring the proximity of the side chains to the HAP surface, we also studied dynamic behavior of the two different phenyl rings with a view to compare the motion of the F7 ring, which is oriented away from the surface, to the motion of the F14 ring, which is oriented toward the surface. CSA and ^{13}C $T_{1\rho}$ measurements have both been used to probe molecular motions. Frey et al. demonstrated that the ^{13}C CSA powder pattern shows a similar CSA for an immobile ring and a 2-fold π-flipping motion, and a drastically reduced CSA for a free rotation.[42] In all cases here—free phenylalanine, free peptides, and HAP-bound peptides—there is large CSA, indicating either immobile rings or a 2-fold π-flip. While large reductions in CSA were previously observed for carbonyls at I11 and G12 for hydrated HAP-bound SN-15,[19] we did not see such large reductions in the side chain CSA for the phenyl ring of F14. These observations are not mutually exclusive, and similar observations have been reported in the literature. For example, Klein et al. studied CSAs of ^{13}C spins in aromatic copolyesters and noted that, with increasing temperature, the CSA of the main chain carbonyl spin was substantially averaged, while the CSA of a nearby main chain aromatic group was only slightly averaged.[38] The authors concluded that, although these observations did not clarify the detailed nature of the carbonyl motions, they did confirm that these two main chain groups do not move as a rigid entity.

In the present context, we observe that the side chain phenyl ring of F14 and the backbone carbonyls of I11 and G12 similarly need not move as a rigid body. Although the common expectation for a native protein is for amino acid side chains to be more mobile than the peptide backbone, the dynamics of SN-15 reflect the influence of the HAP surface. Motions around the $C_\alpha-C_\beta$ and $C_\beta-C_1$ bonds of the phenylalanine side chain as well as local motions of the peptide backbone allows the phenyl ring of F14 to remain partly immobilized on the surface and at the same time leaves the backbone carbonyls of I11 and G12 able to execute larger amplitude reorientations.

We can also probe the frequency of the motions of the phenyl rings of the bound peptides and correlate these to the surface proximity. ^{13}C $T_{1\rho}$ values were measured under three different conditions—hydrated and at 20 °C, hydrated and at −30 °C, and lyophilized and at 20 °C. Data are listed in Table 2. As conditions are applied that will reduce the overall correlation time of the bound peptides, such as reducing temperature and removing water, the F7 ^{13}C $T_{1\rho}$ value decreases, whereas the F14 ^{13}C $T_{1\rho}$ value increases. Increases in line width as these changes are made corroborate the expected reduction in correlation time. The overall relationship between $T_{1\rho}$ and correlation time is

$$\frac{1}{T_{1\rho}} = \frac{\gamma^2 H_z^2 \tau_0}{1 + \omega_1^2 \tau_0^2} + \frac{\gamma^2 (H_x^2 + H_y^2)\tau_0}{2(1 + \omega_0^2 \tau_0^2)}$$

where γ is the gyromagnetic ratio of the specific nucleus, ω_1 is the spin-locking field, ω_0 is the Larmor frequency, τ_0 is the correlation time, and H_z, H_x, and H_y are the fluctuations of the spin locking field in the *x*, *y*, and *z* directions, respectively.[67] Because $\omega_0 \gg \omega_1$, the first term dominates the $T_{1\rho}$ calculation, and we will drop the second term in our analysis of the $T_{1\rho}$

(66) Doig, A. J. *Biophys. Chem.* **2002**, *101*−*102*, 281−293.

(67) Olivieri, A. *Conc. Magn. Reson.* **1998**, *10*, 157−166.

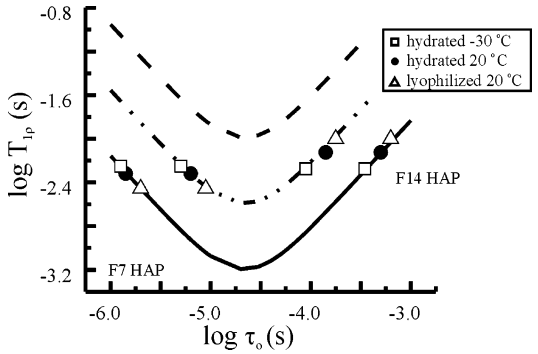

Figure 8. A plot of log(^{13}C $T_{1\rho}$) against log(τ_0) is shown for various values of γH_z. The solid line represents calculation for $\gamma H_z = 12\,000$ Hz; the dotted and dashed line represents a calculation for $\gamma H_z = 6000$ Hz, and the dashed line represents a calculation for $\gamma H_z = 3000$ Hz. Error is contained within the symbols.

data. $T_{1\rho}$ and ω_1 are measured values, τ_0 is the variable we are interested in extracting, and H_z is an unknown value. To probe the correlation time of the phenyl rings, different values of H_z were utilized to create log($T_{1\rho}$) versus log(τ_0) plots. A series of plots is shown in Figure 8, where correlation times are assigned based on the measured $T_{1\rho}$ value and the assumed value for H_z. With a value of $\gamma H_z = 6000$ Hz, a reasonable plot placing the F7 ring dynamics in the high-frequency regime and the F14 ring dynamics in the low-frequency regime can be constructed. At much lower values of γH_z, the minimum does not reach the ^{13}C $T_{1\rho}$ values observed, and at much higher values of γH_z, the separation between the two regimes increases drastically. A lower limit of $\gamma H_z = 5200$ Hz can be assigned based on the ^{13}C $T_{1\rho}$ values obtained. This change between the two regimes suggests that the phenyl ring in the F7 position remains in a two-site jump upon SN-15 binding to the surface, whereas the weak interaction of the F14 ring with the HAP surface hinders the two-site jump of the phenyl ring in that position. These dynamics data are therefore consistent with the REDOR data demonstrating that the F14 ring weakly interacts with the surface. In addition, this weak interaction at the C-terminus compared to the strong interaction of the acidic pentapeptide region allows for the previously observed backbone dynamics.

Conclusion

We have used REDOR NMR to show that, in SN-15, the phenyl ring in the side chain of F14 interacts with the HAP surface, and the plane of this phenyl ring is oriented parallel to the HAP surface. In contrast to F14, REDOR data showed that the phenyl ring of F7 does not interact with the HAP surface. We also used ^{13}C $T_{1\rho}$ measurements to show that the phenyl ring oriented toward the surface is in the low-frequency regime, whereas the phenyl ring oriented away from the surface is in the high-frequency regime, suggesting that the ring pointed away from the surface still undergoes a two-site jump upon binding, whereas the motion of the phenyl ring oriented toward the surface is more hindered. A new model for SN-15 bound to HAP consistent with the data suggests that pS2, pS3, K6, and F14 side chains point to the surface and F7 points away from the surface, and indicates that some of the aromatic amino acid side chains in statherin may be involved in interactions with the HAP surface. Further studies involving the side chains in the full-length statherin and a greater exploration of the role of interfacial water in the protein−HAP binding complex are underway.

Acknowledgment. This work was supported by the NSF (Grants EEC 9529161 and DMR 0110505) and the National Dental Institute (Grant DE-12554). J.M.G. acknowledges support from a NIDCR Training Grant (DE-07023). We thank Torgny Karlsson for developing NMR processing software used in this work, and Greg Olsen and Gil Goobes for useful discussions and help with coding of SIMPSON files. The data obtained on the 7.4 T Chemagnetics Spectrometer were performed at EMSL, a national scientific user facility sponsored by the DOE's Office of Biological and Environmental Research and located at PNNL.

JA056731M